nature energy

Article

https://doi.org/10.1038/s41560-023-01227-6

# Co-deposition of hole-selective contact and absorber for improving the processability of perovskite solar cells

In the format provided by the authors and unedited

# Table of Contents

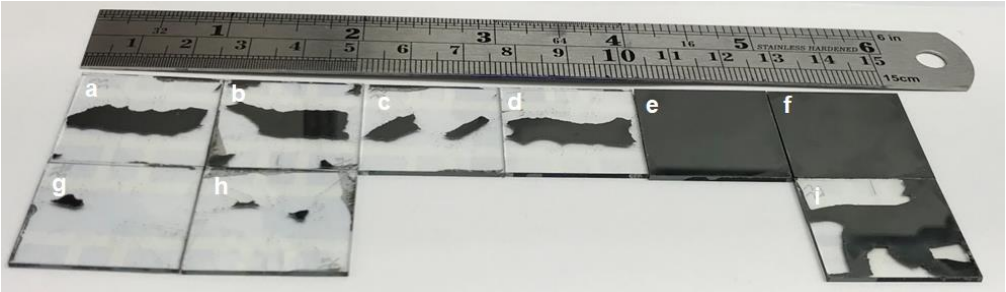


**Supplementary Figure 1. Photographic images of perovskite films processed with different conditions showing wettability issues with certain SAMs.**

**(a)** ITO/Me-4PACz SAM/neat perovskite. 0.5 mg/mL Me-4PACz in ethanol was spin-coated on ITO substrate at 4000 rpm for 30 s and annealed at 100 °C for 10 min. The neat perovskite film was spin-coated on ITO/SAM at 2000 rpm for 2 s and 4000 rpm for 20 s.

**(b)** ITO/Me-4PACz SAM/neat perovskite. 0.5 mg/mL Me-4PACz in ethanol was spin-coated on ITO substrate at 4000 rpm for 30 s and annealed at 100 °C for 10 min. The neat perovskite film was spin-coated on ITO/SAM at 4000 rpm for 22 s.

**(c)** ITO/Me-4PACz SAM/neat perovskite. 1 mg/mLMe-4PACz in ethanol was spin-coated on ITO substrate at 4000 rpm for 30 s and annealed at 100 °C for 10 min. The neat perovskite film was spin-coated on ITO/SAM at 2000 rpm for 2 s and 4000 rpm for 20 s.

**(d)** ITO/Me-4PACz SAM/neat perovskite. 1 mg/mL Me-4PACz in ethanol was spin-coated on ITO substrate at 4000 rpm for 30 s and annealed at 100 °C for 10 min. The neat perovskite film was spin-coated on ITO/SAM at 4000 rpm for 22 s.

**(e)** ITO/neat perovskite. The neat perovskite film was spin-coated on ITO at 2000 rpm for 2 s and 4000 rpm for 20 s.

**(f)** ITO/target perovskite processed with 0.5 mg/mL Me-4PACz in precursor. The target perovskite film was spin-coated on ITO at 2000 rpm for 2 s and 4000 rpm for 20 s.

**(g)** ITO/Me-4PACz SAM/neat perovskite washed off/ redeposited neat perovskite. The perovskite film processed with the same condition in panel A was washed off with DMF and redeposited neat perovskite at 2000 rpm for 2 s and 4000 rpm for 20 s.

**(h)** ITO/Me-4PACz SAM/neat perovskite washed off/ redeposited neat perovskite. The perovskite film processed with the same condition in panel B was washed off with DMF and redeposited neat perovskite at 2000 rpm for 2 s and 4000 rpm for 20 s.

**(i)** ITO/target perovskite washed off/ redeposited neat perovskite. The perovskite film processed with the same condition in panel F was washed off with DMF and redeposited neat perovskite at 2000 rpm for 2 s and 4000 rpm for 20 s.

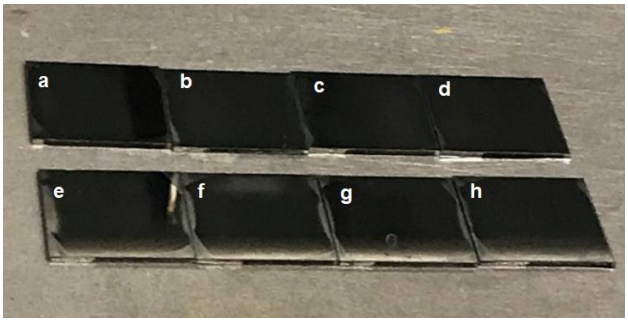


**Supplementary Figure 2. Photographic images of perovskite films processed with different conditions.** (**a** to **d**) Photographic images of ITO/perovskite processed with 0.5 mg/mL 2PACz in the precursor. The perovskite film was spin-coated on ITO at 2000 rpm for 2 s and 4000 rpm for 20 s. (**e** to **h**) Photographic images of ITO/2PACz SAM/neat perovskite. 1 mg/ml 2PACz in ethanol was spin-coated on ITO substrate at 4000 rpm for 30 s and the neat perovskite film was spin-coated on ITO/SAM at 2000 rpm for 2 s and 4000 rpm for 20 s.

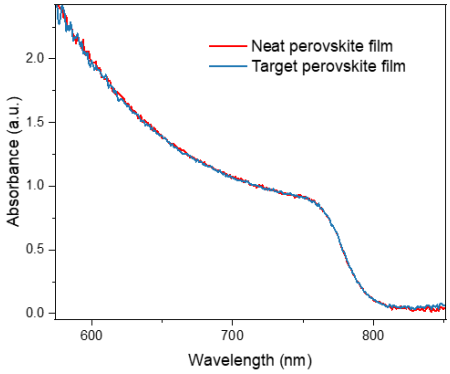


**Supplementary Figure 3. UV-Vis absorption spectra for neat and target perovskite films.** UV-Vis absorption spectra for the neat perovskite film and the target perovskite film processed with Me-4PACz in precursor.

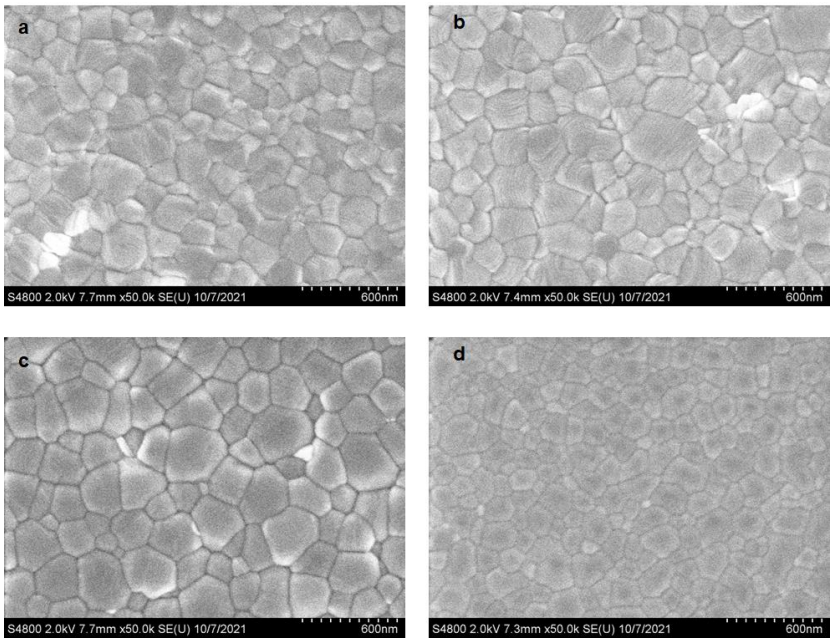


**Supplementary Figure 4. The morphology of perovskite films processed with different Me-4PACz concentrations in precursor.** SEM images of (**a**) neat perovskite film, (**b**) perovskite film processed with 0.5 mg/mL Me-4PACz in precursor, (**c**) perovskite film processed with 1 mg/mL Me-4PACz concentrations in precursor, and (**d**) perovskite film processed with 2 mg/mL Me-4PACz in precursor.

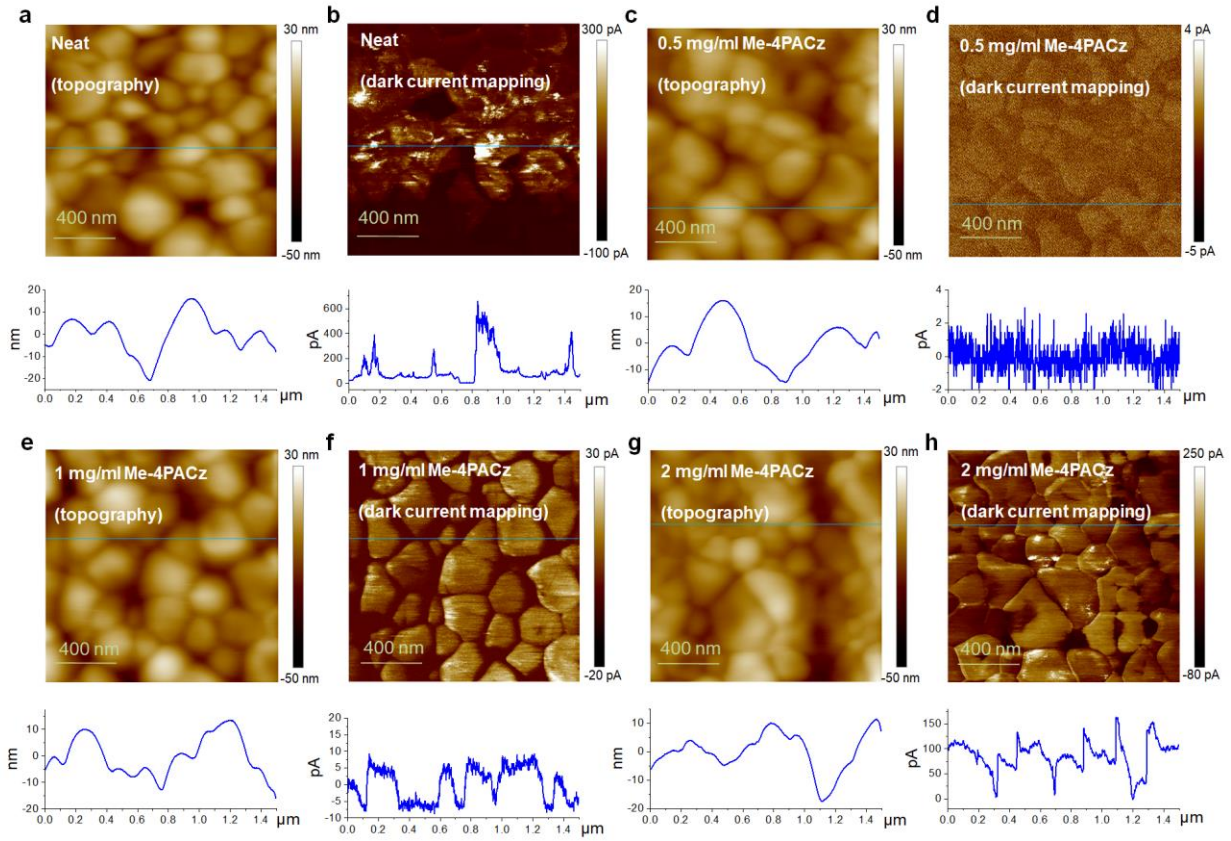


**Supplementary Figure 5. AFM topography images and c-AFM dark current mapping of perovskite films processed with different Me-4PACz concentrations in precursor.** AFM topography images (**a**) and c-AFM dark current mapping (**b**) of neat perovskite film. AFM topography images (**c**) and c-AFM dark current mapping (**d**) of perovskite film processed with 0.5 mg/mL Me-4PACz in precursor. AFM topography images (**e**) and c-AFM dark current mapping (**f**) of perovskite film processed with 1 mg/mL Me-4PACz in precursor. AFM topography images (**g**) and c-AFM dark current mapping (**h**) of perovskite film processed with 2 mg/mL Me-4PACz in precursor.

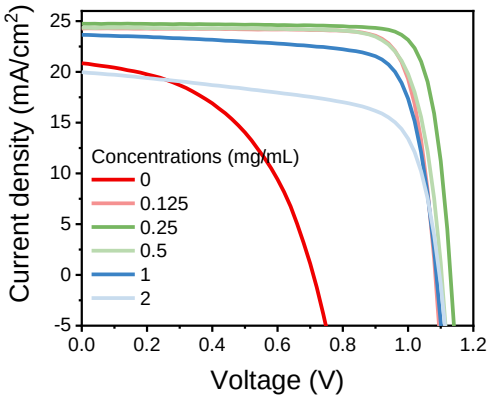


**Supplementary Figure 6. Me-4PACz concentration-dependent J-V characteristics of 1.55 eV PSCs.** Me-4PACz concentration-dependent device *J-V* characteristics for $Cs_{0.05}(FA_{0.98}MA_{0.02})_{0.95}Pb(I_{0.98}Br_{0.02})_3$ ($E_G$ ~1.55 eV) devices with and without Me-4PACz in precursor.

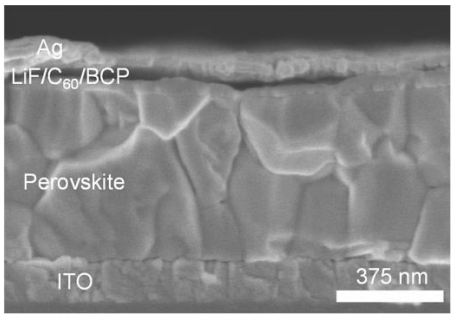


**Supplementary Figure 7. SEM cross-section image of target 1.56 eV PSC.** SEM cross-section image of a target $Cs_{0.05}(FA_{0.92}MA_{0.08})_{0.95}Pb(I_{0.92}Br_{0.08})_3$ ($E_G$ ~1.56 eV) PSC (without surface passivation treatment) processed with 0.5 mg/mL Me-4PACz in precursor.

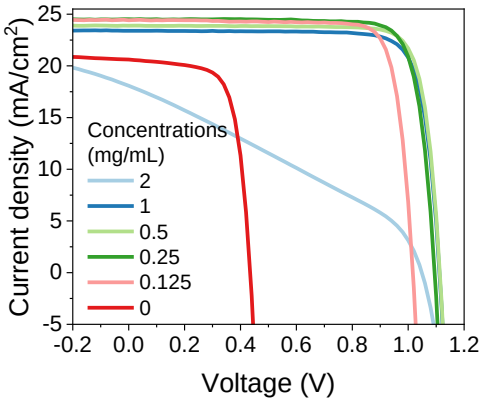


**Supplementary Figure 8. Me-4PACz concentration-dependent J-V characteristics of 1.56 eV PSCs.** Me-4PACz concentration-dependent device *J-V* characteristics for $Cs_{0.05}(FA_{0.92}MA_{0.08})_{0.95}Pb(I_{0.92}Br_{0.08})_3$ ($E_G$ ~1.56 eV) devices with and without Me-4PACz in precursor.

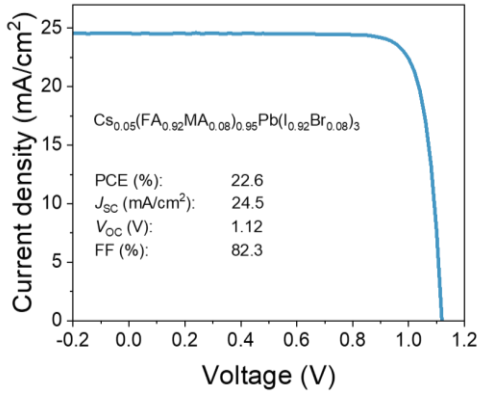


**Supplementary Figure 9. PV performance of target 1.56 eV PSC.** *J-V* curve of a target $Cs_{0.05}(FA_{0.92}MA_{0.08})_{0.95}Pb(I_{0.92}Br_{0.08})_3$ ($E_G$ ~1.56 eV) PSC fabricated with 0.5 mg/mL Me-4PACz in perovskite precursor.

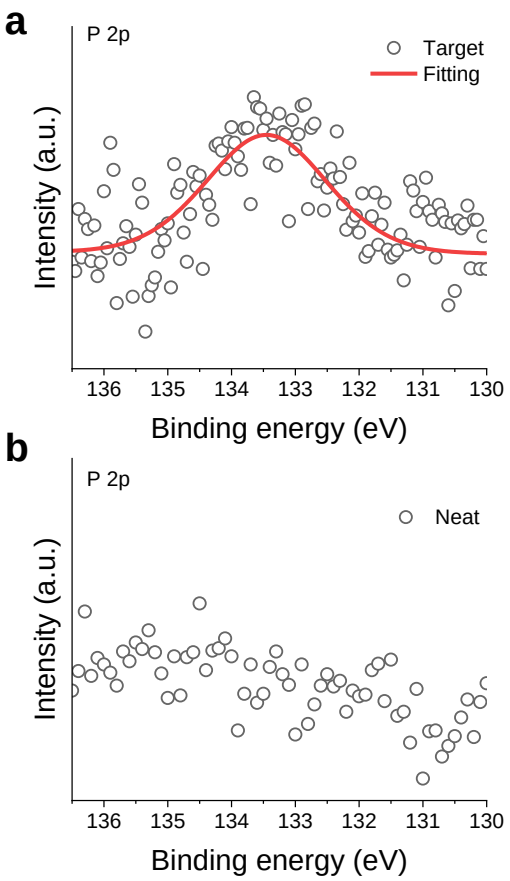


**Supplementary Figure 10. XPS spectra for P 2p on ITO-coated substrates with neat or target perovskite film removed.** The perovskite films with (target) or without (neat) Me-4PACz were cast and then removed with DMF. (**a**, **b**) XPS spectra for P 2p on ITO substrates with the target perovskite film and neat perovskite film washed off, respectively.

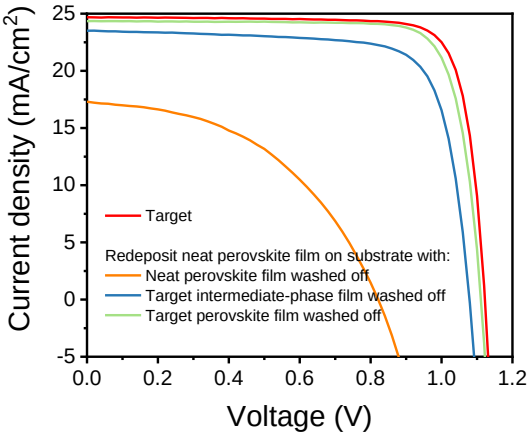


**Supplementary Figure 11. PV performance of neat PSCs (1.55 eV) fabricated on the substrates with intermediate-phase/perovskite film washed off.** *J-V* characteristics of the neat PSCs (1.55 eV) fabricated on substrates with intermediate-phase/perovskite film washed off.

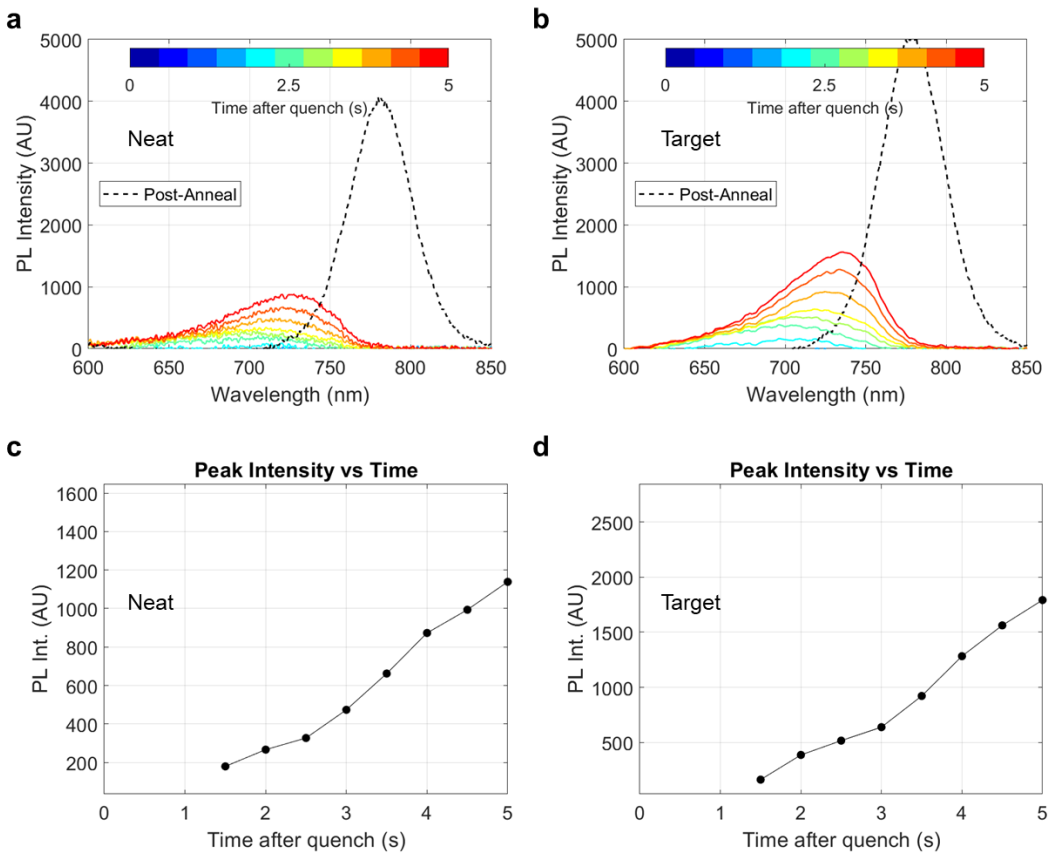


**Supplementary Figure 12. In situ observation of PL evolution of neat and target perovskite film during the crystallization process.** (**a**, **b**) The evolution of PL intensity after quench (antisolvent dropping) of neat (a) and target (b) perovskite films, respectively. The *in situ* PL was measured on the spin-coater with a custom-built fiber optic-based PL spectrometer. (**c**, **d**) The evolution of PL intensity vs. time after quench (antisolvent dropping) of neat (c) and target (d) perovskite films, respectively.

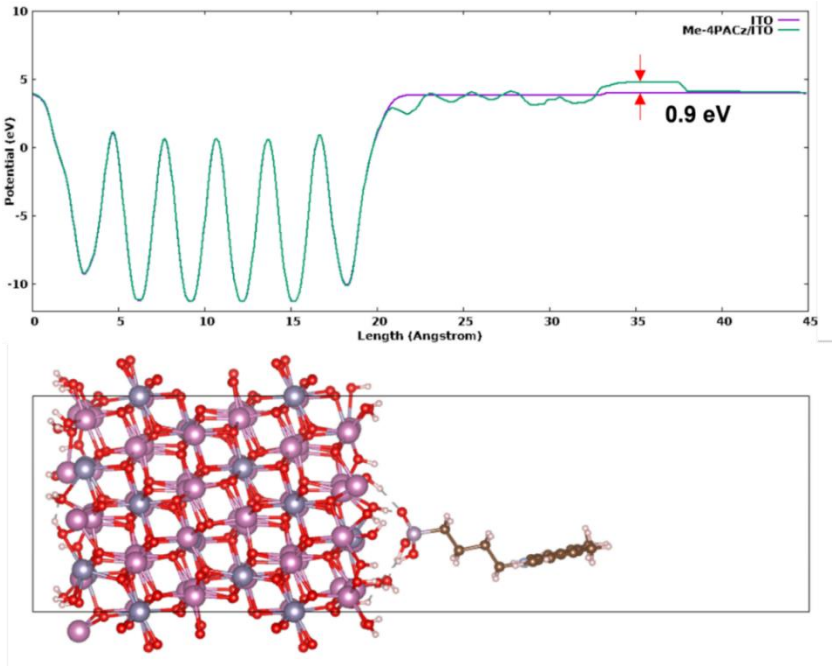


**Supplementary Figure 13. The electrostatic potential and crystal structure of ITO/Me-4PACz interface.** Planar averaged electrostatic potential (top) and crystal structure (bottom) of the ITO/Me-4PACz interface calculated by DFT.

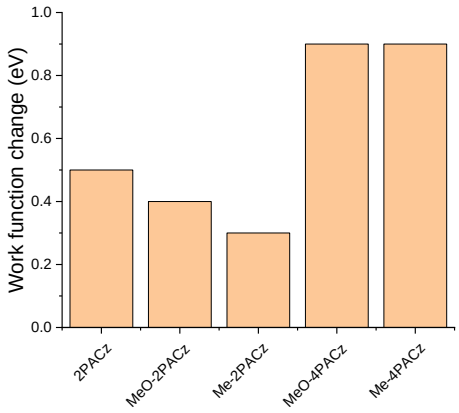


**Supplementary Figure 14. Work function changes of SAM modified ITO calculated by DFT.** Changes in work function as evaluated by DFT for ITO substrate with modification by different phosphonic acids.

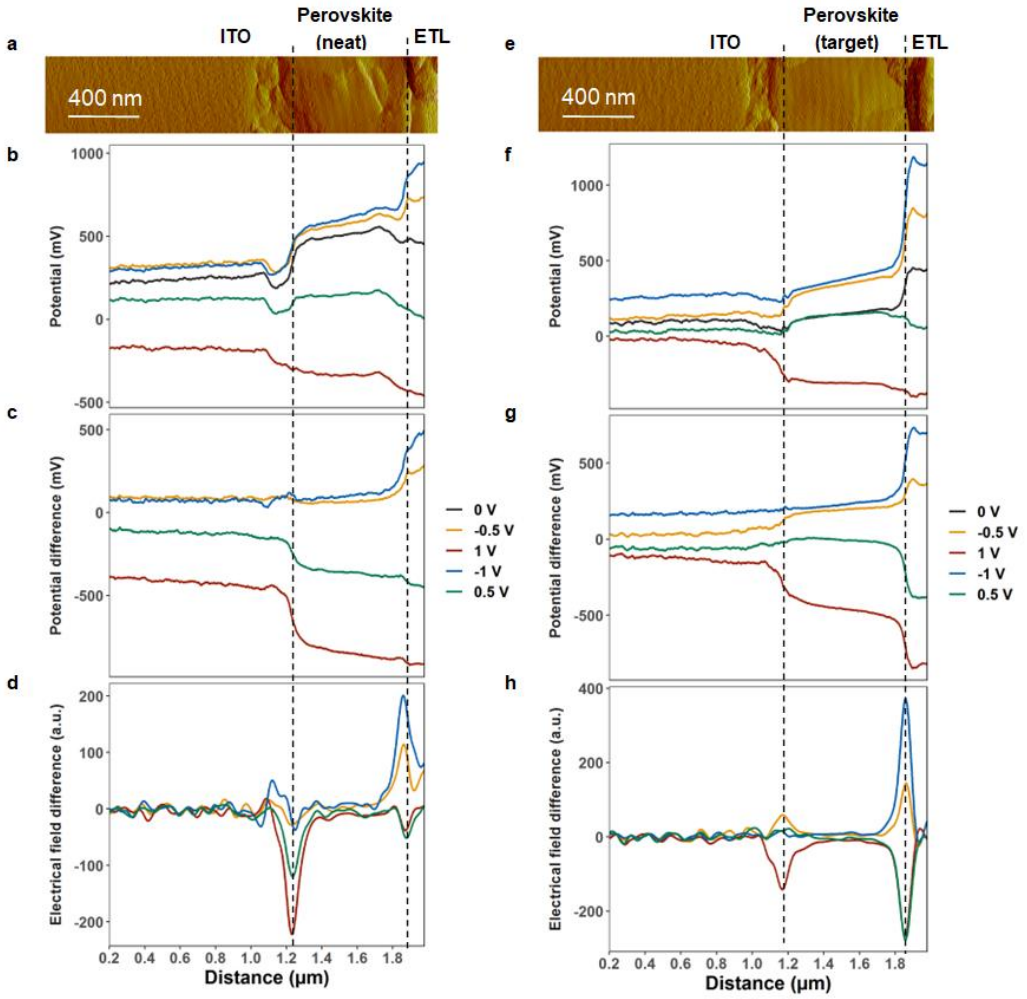


**Supplementary Figure 15. Kelvin probe force potential profiling of solar cell devices.** (**a**) AFM image of a cross-section of control perovskite device. (**b** to **d**) Potential profiling (b), potential difference (c), and electrical field difference (d) of neat perovskite device. (**e**) AFM image of a cross section of target perovskite device. (**f** to **h**) Potential profiling (f), potential difference (g), and electrical field difference (h) of target perovskite device.

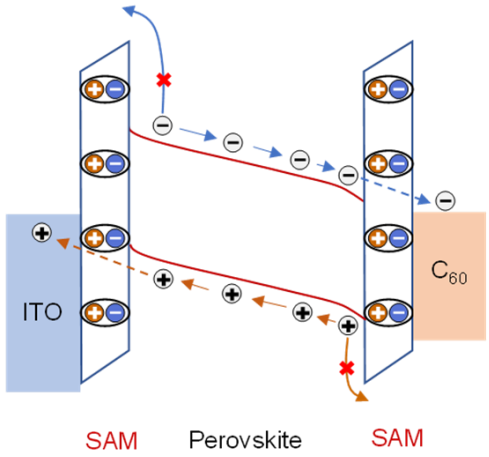


**Supplementary Figure 16. Band diagram of the target PSCs under short-circuit condition.**

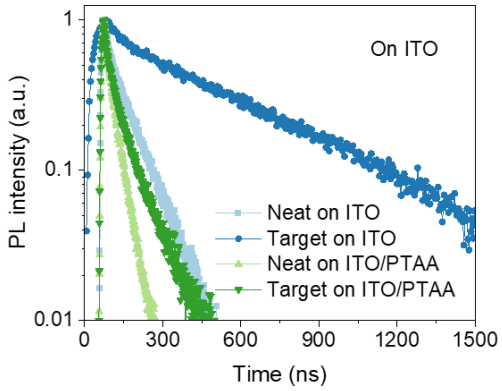


**Supplementary Figure 17. TRPL of perovskite films on ITO and ITO/PTAA substrates.**

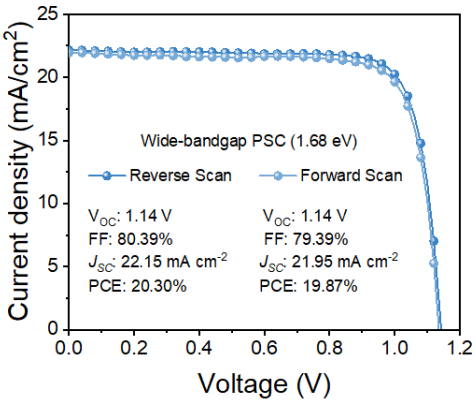


**Supplementary Figure 18. PV performance of target wide bandgap (1.68 eV) PSCs without surface passivation.** *J-V* curves of the target wide bandgap (1.68 eV) PSCs without surface passivation treatment fabricated with Me-4PACz in perovskite precursor.

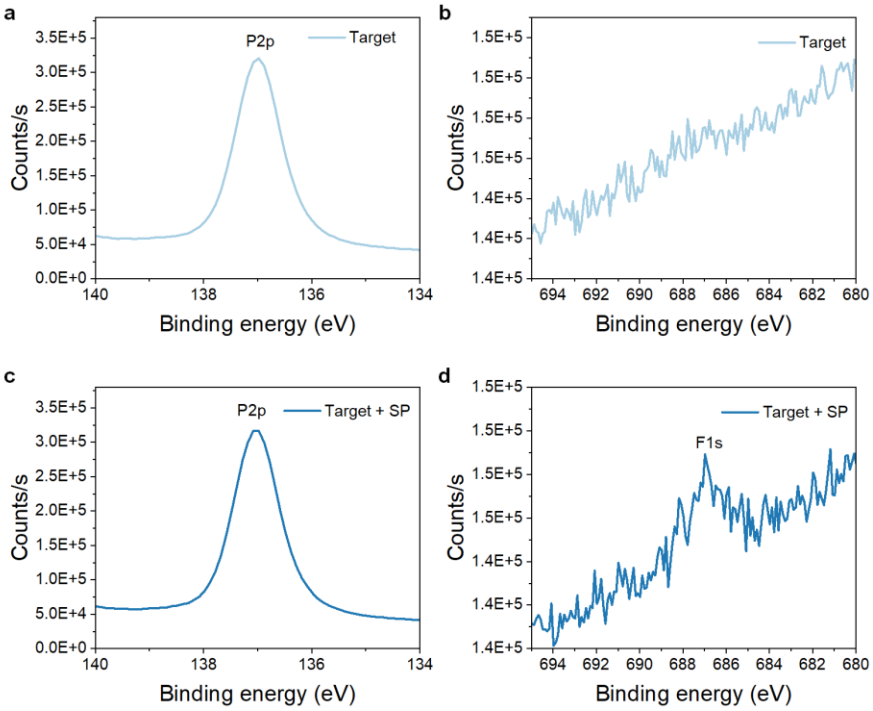


**Supplementary Figure 19. XPS spectra for P2p and F1s on target perovskite film with and without surface passivation.** (**a**, **b**) XPS spectra for P2p and F1s on target perovskite film. (**c**, **d**) XPS spectra for P2p and F1s on target perovskite film with $CF_3$-PEAI and MAI surface passivation. SP: surface passivation.

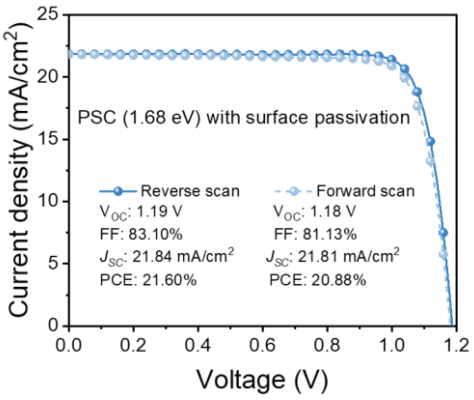


**Supplementary Figure 20. PV performance of target wide bandgap (1.68 eV) PSCs with surface passivation.** *J-V* curves of the target wide bandgap (1.68 eV) PSCs with surface passivation treatment fabricated with Me-4PACz in perovskite precursor.

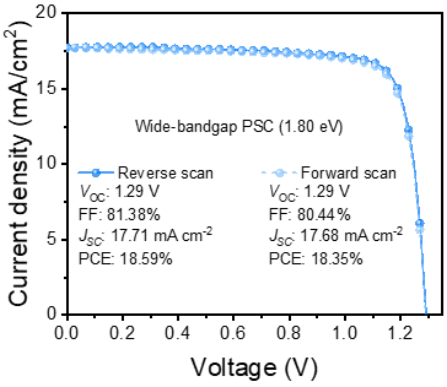


**Supplementary Figure 21. PV performance of target 1.8 eV PSCs with surface passivation.** *J-V* curves of the target $Cs_{0.15}FA_{0.85}Pb(I_{0.6}Br_{0.4})_3$ 1.8 eV PSCs with surface passivation fabricated with Me-4PACz in perovskite precursor.

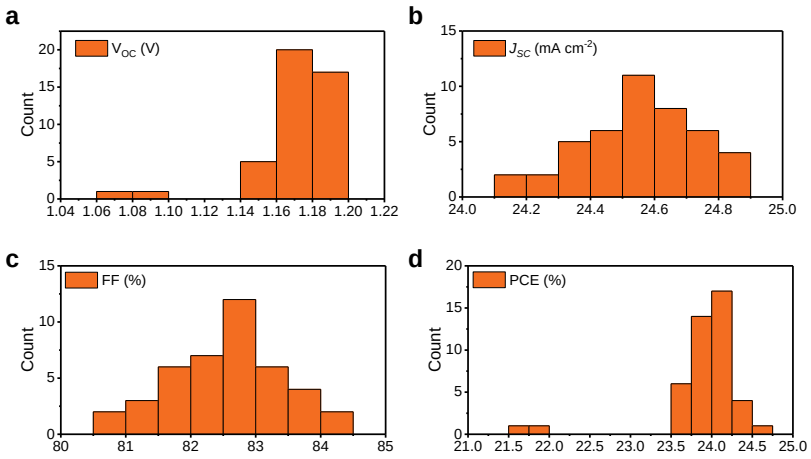


**Supplementary Figure 22. The PV parameters distribution of 44 target 1.55 eV devices with surface passivation.** (**a**) $V_{OC}$, (**b**) $J_{SC}$, (**c**) FF, (**d**) PCE.

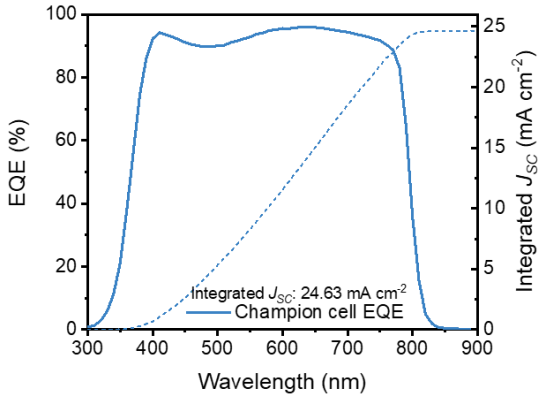


**Supplementary Figure 23. EQE spectrum of the target champion PSC.** EQE spectrum of the champion 1.55 eV device with surface passivation.

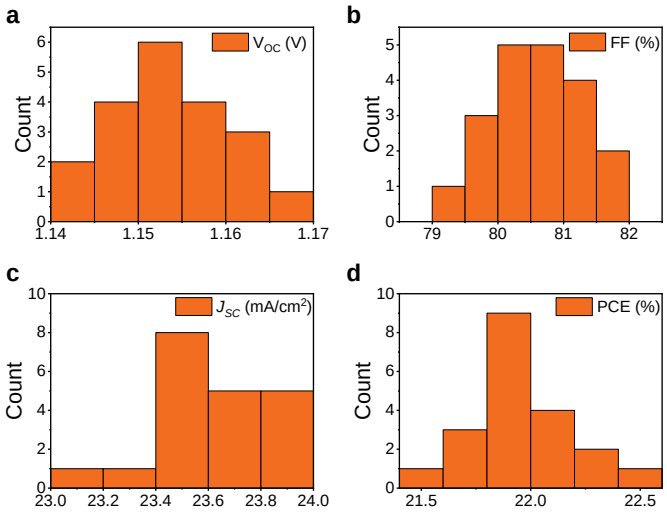


**Supplementary Figure 24. The PV parameters distribution of 20 blade-coated (1-cm$^2$) 1.55 eV devices with surface passivation.** (**a**) $V_{OC}$, (**b**) FF, (**c**) $J_{SC}$, (**d**) PCE.

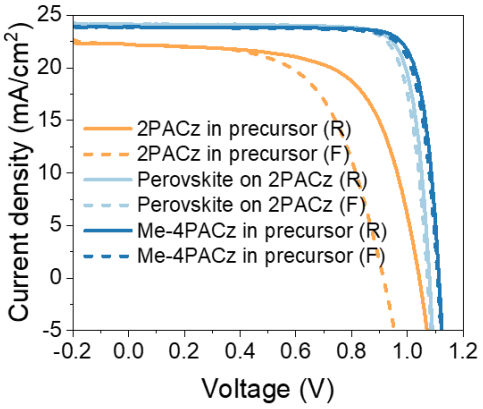


**Supplementary Figure 25. PV performance of PSCs fabricated with 2PACz or Me-4PACz in precursor.** *J-V* curves from both forward (F) and reverse (R) scan of the perovskite devices on ITO/2PACz, and perovskite devices fabricated with 2PACZ and Me-4PACz in the perovskite precursor.

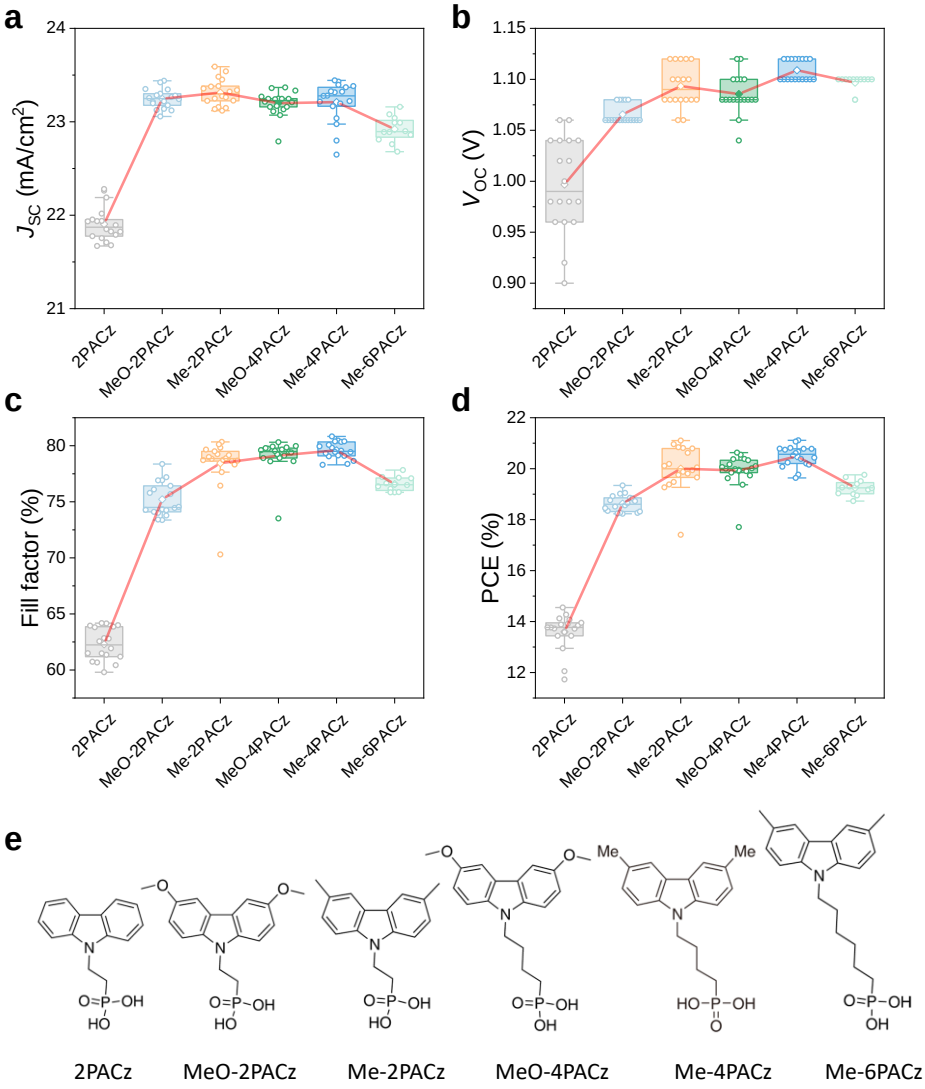


**Supplementary Figure 26. PV parameters analysis for 102 devices fabricated with different phosphonic acids in perovskite precursor.** (**a**) $J_{SC}$, (**b**) $V_{OC}$, (**c**) FF, (**d**) PCE, (**e**) Chemical structure of different phosphonic acids. The box plots in **a**–**d** show the mean, median line, and 25%~75% box limits with 1.5x interquartile range whiskers. The mean values are connected to show the trend. The number of samples measured for the PSCs with 2PACz, MeO-2PACz, Me-2PACz, MeO-4PACz, Me-4PACz, and Me-6PACz is 18, 18, 18, 18, 18, and 12, respectively.

**Supplementary Table 1. Extracted TRPL lifetime of Fig. 2h.** Bi-exponential fitting method with the equation $y(t) = A_1\exp(-t/\tau_1) + A_2\exp(-t/\tau_2) + y_0$ was used. The average lifetime can be calculated with the equation $\tau_{avg} = (A_1\tau_1^2 + A_2\tau_2^2)/(A_1\tau_1 + A_2\tau_2)$.

| Samples | $\tau_1$ (ns) | $\tau_2$ (ns) | $\tau_{ave}$ (ns) |
|---|---|---|---|
| Neat | 49.1 | 372.7 | 304.95 |
| 0.5 mg/ml | 56.1 | 589.8 | 520.46 |
| 2 mg/ml | 40.4 | 487.3 | 416.64 |

**Supplementary Table 2. Extracted TRPL lifetime of Supplementary Fig. 17.** Bi-exponential fitting method with the equation $y(t) = A_1\exp(-t/\tau_1) + A_2\exp(-t/\tau_2) + y_0$ was used.

| Samples | $\tau_1$ (ns) | $\tau_2$ (ns) |
|---|---|---|
| Neat on ITO | 12.8 | 98.5 |
| Target on ITO | 79.8 | 614.8 |
| Neat on ITO/PTAA | 13.2 | 43.5 |
| Target on ITO/PTAA | 10.2 | 70.1 |

**Supplementary Table 3. Summary of high-performance inverted PSCs.**

| Year | HTL/HSC and perovskite fabrication method | PCE | MPP-stability | Ref. |
|---|---|---|---|---|
| 2017 | Two-step (layer by layer) | 21.0% | 86% of initial PCE, 26 hour | [1] |
| 2018 | Two-step (layer by layer) | 21.5% | No loss, 20 hour | [2] |
| 2020 | Two-step (layer by layer) | 23.0% | No loss, 1000 hour | [3] |
| 2022 | Two-step (layer by layer) | 23.91% | No loss, 1000 hour | [4] |
| 2022 | Two-step (layer by layer) | 24.3% | >90% of initial PCE, 1000 hour | [5] |
| 2022 | Two-step (layer by layer) | 25.0% | >98% of initial PCE, 1500 hour | [6] |
| 2022 | Two-step (layer by layer) | 25.37% | >87% of initial PCE, 2400 hour | [7] |
| **2022** | **One-step** | **24.5%** | **>90% of initial PCE, 1200 hour** | **this work** |

**Note:** "HTL" represents hole-transport layer; "HSC" represents hole-selective contact; "Two-step (sequential)" represents depositing HTL/HSC and perovskite sequentially; "One-step" represents depositing HTL/HSC and perovskite simultaneously in one coating procedure.

**Supplementary Table 4. Summary of the photovoltaic parameters of 44 target 1.55 eV PSCs with surface passivation.** The parameters listed in parentheses are the maximum values. The plus-minus sign (±) represents the standard deviation.

| $V_{OC}$ (V) | FF (%) | $J_{SC}$ (mA/cm$^2$) | PCE (%) |
|---|---|---|---|
| 1.18±0.02 (1.19) | 82.59±0.96 (84.15) | 24.59±0.18 (24.89) | 23.87±0.52 (24.50) |

**Supplementary References**


1. Zheng, X. et al. Defect passivation in hybrid perovskite solar cells using quaternary ammonium halide anions and cations. *Nat. Energy* **2**, 17102 (2017).
2. Luo, D. et al. Enhanced photovoltage for inverted planar heterojunction perovskite solar cells. *Science* **360**, 1442-1446 (2018).
3. Zheng, X. et al. Managing grains and interfaces via ligand anchoring enables 22.3%-efficiency inverted perovskite solar cells. *Nat. Energy* **5**, 131-140 (2020).
4. Chen, H. et al. Quantum-size-tuned heterostructures enable efficient and stable inverted perovskite solar cells. *Nat. Photon.* **16**, 352-358 (2022).
5. Li, X. et al. Constructing heterojunctions by surface sulfidation for efficient inverted perovskite solar cells. *Science* **375**, 434-437 (2022).
6. Li, Z. et al. Organometallic-functionalized interfaces for highly efficient inverted perovskite solar cells. *Science* **376**, 416-420 (2022).
7. Jiang, Q. et al. Surface reaction for efficient and stable inverted perovskite solar cells. *Nature* **611**, 278-283 (2022).